Icarus 277 (2016) 311–318

Contents lists available at ScienceDirect

Icarus

journal homepage: www.elsevier.com/locate/icarus

The diurnal libration and interior structure of Enceladus

Tim Van Hoolst[a,b,*], Rose-Marie Baland[c,a], Antony Trinh[a]

[a] Royal Observatory of Belgium, Ringlaan 3, Brussels B-1180, Belgium
[b] Instituut voor Sterrenkunde, KU Leuven, Celestijnenlaan 200D, Leuven B-3001, Belgium
[c] Georges Lemaître Centre for Earth and Climate Research, Earth and Life Institute, Université catholique de Louvain, Place Louis Pasteur, 3, Louvain-la-Neuve B-1348, Belgium

ARTICLE INFO

Article history:
Received 22 December 2015
Revised 11 May 2016
Accepted 13 May 2016
Available online 24 May 2016

Keywords:
Enceladus
Interiors
Rotational dynamics

ABSTRACT

We determine constraints on the ice shell and ocean of Enceladus from the observed libration at orbital period by assessing the effects of uncertainties in the size, density, rigidity, and viscosity of the internal layers and of the non-hydrostatic structure on the libration. The observed libration amplitude implies that the average thickness of the ice shell is between 14 km and 26 km and that the ocean is 21 km to 67 km thick.

1. Introduction

The gravitational force exerted by Saturn on Enceladus raises tides that are thought to be responsible for the observed geyser activity at the south pole of Enceladus (Porco, 2006; Spencer et al., 2006). Although the precise cause and mechanism of cryovolcanism is not well understood, the variation of the plume intensity and its correlation with the orbital position of Enceladus is strongly indicative of a tidal mechanism driving the geysers (Hedman et al., 2013; Hurford et al., 2007; Porco et al., 2014). The detection of sodium-salt-rich ice grains emitted from the plume suggests that the plume is connected to a subsurface salty water reservoir in contact with silicate rocks (Hsu et al., 2015; Postberg et al., 2009; 2011). The subsurface ocean might exist only beneath the region of activity near to the south polar region (Tobie et al., 2008), although recent gravity and topography data cannot distinguish between a local and a global subsurface ocean (Iess et al., 2014; McKinnon, 2015).

The gravitational interaction with Saturn also periodically changes the rotation of Enceladus, which might be co-responsible for the observed variations in plume activity (Nimmo et al., 2014a). The diurnal librations of Enceladus, representing the variations at orbital period in the rotation angle with respect to the steady change for a constant rotation rate, have recently been accurately determined by a detailed analysis of images of Enceladus taken by the Cassini imaging system (Thomas et al., 2016). Although the libration amplitude of 0.120 ± 0.014 degree (2σ) is too small for diurnal libration to play an important role in the variation in tidal stress needed to explain the plume variability (Nimmo et al., 2014b), it provides unique direct insight into the interior structure through the sensitivity of libration to the existence and certain characteristics of a liquid global internal layer. Thomas et al. (2016) showed that the libration amplitude proves the existence of a global ocean beneath an icy surface.

Here we perform an extended study of the diurnal librations of Enceladus in order to determine the best constraints on ice shell and ocean, in particular on the mean thickness of the ice shell. We study the effect of the rigidity and visco-elastic behavior of the ice shell on the librations and assess the uncertainty they introduce in the interpretation of the libration amplitude in terms of the depth to the ocean. We first use an approach in which Enceladus is considered to be in hydrostatic equilibrium. Next, we use the observed topography and gravitational field of Enceladus to develop non-hydrostatic models of the interior structure. Two different end-member assumptions are considered for the shape of the interfaces between the core, the ocean and the ice shell. By means of those models, we then investigate the librations for non-hydrostatic models of Enceladus that are consistent with gravity and topography data (Iess et al., 2014; Nimmo et al., 2011). We show that although many uncertainties remain about Enceladus' interior structure, the mean thickness of the ice shell can be well constrained by the libration amplitude.

2. Libration without global subsurface ocean

The gravitational torque of Saturn exerted on Enceladus forces the rotation of Enceladus to vary slightly during the orbital motion.

* Corresponding author at: Royal Observatory of Belgium, Ringlaan 3, B-1180 Brussels, Belgium. Tel.: 32 23730668.
E-mail address: tim.vanhoolst@oma.be (T.V. Hoolst).

http://dx.doi.org/10.1016/j.icarus.2016.05.025
0019-1035/

Since Enceladus is likely in a 1:1 spin-orbit resonance, the torque will have periods commensurate with the orbital period, which is equal to the rotation period of Enceladus, and will force librations with the same periods. In addition, Enceladus has librations with longer periods related to the variations in the torque associated with periodic perturbations of the orbit of Enceladus due to Dione. The two main long-period librations have periods of about 4 and 11 years (Rambaux et al., 2010). Since the observations of Thomas et al. (2016) have a period equal to the orbital period, we neglect those long-period librations here.

The polar gravitational torque leading to variations in the rotation rate can be expressed in terms of the external gravitational field coefficients of Enceladus (e.g. Dehant and Mathews, 2015), which have been determined up to degree 3 by Iess et al. (2014). Six gravitational coefficients have been estimated, all five of degree two (J_2, C_{21}, S_{21}, C_{22}, S_{22}) and the zonal component of degree three (J_3), but only the torque on C_{22} needs to be taken into account.The polar torque does not depend on the zonal gravitational coefficients because of the geometric symmetry of the zonal harmonics with respect to the polar axis. The contributions of the tesseral coefficients to the polar torque can be neglected since they are approximately proportional to the very small obliquity of Enceladus. The obliquity is not known, but theoretical calculations predict values below 10^{-5} radians (Baland et al., 2014). The S_{22} sectorial coefficient is about 70 times smaller than the C_{22} coefficient (Iess et al., 2014), and its contribution to the gravitational torque is therefore also neglected.

The torque forces libration at the orbital period and at the subharmonic periods of it. The latter will also be neglected as the torque at the nth subharmonic is smaller than that at orbital period by a factor e^n (e.g. Van Hoolst et al., 2008), where $e = 0.0047$ is the orbital eccentricity (Thomas et al., 2016). We introduce the libration angle $\gamma = \phi - M$, where ϕ is the rotation angle of Enceladus and M the mean anomaly. When the libration at orbital period of 1.37 days is written as $\gamma = g\sin(M + \pi)$, the libration amplitude $g_{\rm solid}$ for an entirely solid and elastic Enceladus can be expressed as

$$g_{\rm solid} = 6\frac{\tilde{B} - \tilde{A}}{\tilde{C}}\frac{en^2}{n^2 - \omega_f^2} \approx 6e\frac{\tilde{B} - \tilde{A}}{\tilde{C}}, \quad (1)$$

where ω_f is the frequency of the free libration

$$\omega_f = n\sqrt{\frac{3(B-A)}{\tilde{C}}\frac{k_f - k_2}{k_f}} \quad (2)$$

and $\tilde{B} = B(k_f - 5k_2/6)/k_f$, $\tilde{A} = A(k_f - 5k_2/6)/k_f$ and $\tilde{C} = C + 4k_2n^2R^5/(9G)$ (Van Hoolst et al., 2013). Here $A < B$ are the equatorial principal moments of inertia, C the polar principal moment of inertia, $R = 252.1$ km the radius and G the universal gravitational constant. The mean motion of Enceladus' orbit is denoted by n, k_2 is the classical potential Love number, and k_f the fluid Love number. The libration amplitude of the forced libration at orbital period depends on a free frequency, similarly to a harmonic oscillator, but we assume that the free libration mode is damped as the damping timescale is extremely short compared to the age of the Solar System (see, e.g. Tiscareno et al., 2009).

For the numerical evaluation, we use the degree-two, order-two gravitational coefficient $C_{22} = (B-A)/(4M_ER^2) = (1549.8 \pm 15.6) \times 10^{-6}$, with mass $M_E = 1.0794 \times 10^{20}$ kg, and the estimate of the mean moment of inertia $I = (A+B+C)/3 = (0.335 \pm 0.005)MR^2$ (2 sigma) derived from Radau's equation and the degree-two gravity field of Enceladus (Iess et al., 2014). For an entirely solid Enceladus, k_2 is small and approximately 1.5×10^{-4} depending somewhat on the density and rigidity profile (Baland et al., 2016), and $k_f = (B-A)/(qM_ER^2) \approx 0.989$ with $q = (n^2R^3)/(GM_E)$ the ratio of the centrifugal acceleration to the gravitational acceleration. The free libration period is then 5.81 days (5.77 days for a homogeneous model, Thomas et al., 2016), far enough from the forcing period of 1.37 days for the approximation in Eq. (1) to be valid. Elasticity, which has been included here, lengthens the free period by less than 0.01% since the tides of a solid Enceladus are very small with a radial tidal displacement of the order of a centimeter. A local subsurface ocean will be able to increase the tides, at least locally, but cannot substantially change the free libration period since the shell librates together with the deeper solid interior.

The libration amplitude for a solid and elastic Enceladus is about 132 m at the equator, four times smaller than the observed value of (528 ± 62) m (Thomas et al., 2016). Thomas et al. (2016) argued that the incompatibility of the observation with the libration amplitude of a solid and rigid Enceladus is evidence of a subsurface ocean. Elasticity does not change that conclusion since elasticity decreases the libration amplitude (by less than a meter). Any larger elasticity (smaller rigidity) than assumed here, for example for a porous core as suggested by Hsu et al. (2015), would imply an even smaller libration amplitude and a stronger inconsistency with the observations. Visco-elastic behavior of the ice would also drain energy from libration to deformation and dissipation and will further reduce the libration amplitude.

We conclude that a partially decoupling layer must exist, which allows for differential rotation between different layers of the satellite. Since measurements of the plume composition demonstrate that the water has been in contact with rocks (Postberg et al., 2011), libration strongly suggests that Enceladus is composed of a solid icy outer shell on top of a liquid ocean mainly composed of water that is in contact with a solid core containing silicates in its top layers. A detailed study of the libration of Enceladus with an ocean is presented in the next section.

3. libration with a global subsurface ocean

3.1. Libration model

In order to assess the effect of various interior structure parameters, such as the thickness of the ice shell, on the libration amplitude, and to constrain some of these parameters based on the observed libration, we construct a large set of interior structure models of Enceladus with a global subsurface ocean for which we calculate the libration. All models satisfy the total mass M_E and radius R and have a mean moment of inertia $I/(M_ER^2)$ between 0.325 and 0.345, covering the moment of inertia estimate of Iess et al. (2014) within the two sigma precision ([0.33, 0.34]) and the range [0.328, 0.333] obtained by McKinnon (2015). The ranges of values considered for the radii and densities of the core, ocean and ice shell are given in Table 1. We choose the density of the ice shell to be in the interval [900, 1000] kg/m^3. This range is somewhat larger than the range of [900, 950] kg/m^3, often considered for pure ice including some degree of porosity in studies of the ice shells of icy satellites (e.g. Nimmo et al., 2014a), to include also the effect of the presence of contaminants. For the ocean, we consider a density range of [950,1100] kg/m^3 to include a wide range of salinity values and temperatures. We refer to Sharqawy et al. (2010) for seawater densities on Earth and the online density table at web.mit.edu/seawater/ where water density values are given between 943.1 kg/m^3 and 1096.2 kg/m^3 for temperatures between 0 and 120 °C, atmospheric pressure, and salinities between 0 and 120 g/kg.

The reference models of the interior structure of Enceladus are spherically symmetric. To be able to study the libration, we calculate the degree-two shape of the three interfaces (surface, interface between the ocean and the ice shell, and interface between the core and the ocean). As explained above, libration only depends on the degree-two shape and we therefore consider that the

Table 1
Ranges of values of the parameters of the interior structure of Enceladus for models that satisfy the observed libration amplitude for different modeling hypotheses: rigid models in hydrostatic equilibrium (HE), elastic models in hydrostatic equilibrium with shell rigidity in the range $[10^9, 5 \times 10^9]$ Pa, elastic non-hydrostatic models with compensation at the ocean-shell interface, and elastic non-hydrostatic models with compensation at the core-ocean interface. The mean thickness of the shell h_s and ocean h_o and the mean radius of the core r_c are given in km, the densities in kg m^{-3}. The initial sampling is given in the last column. The sampling interval is 25 kg m^{-3} for the shell and ocean density, 1 km for shell thickness and 5 km for core radius. For the non-hydrostatic case with a non-equipotential ocean-shell interface, the density of the ocean is at the high end since the density difference must be sufficiently large in order to explain the gravity data. The libration amplitudes are calculated by solving Eqs. (45) and (46) of Van Hoolst et al. (2013).

Quantity	Rigid HE	Elastic HE	Non-HE ocean	Non-HE core	Sampling
h_s	[16, 24]	[14, 24]	[14, 24]	[18, 26]	[5, 72]
h_o	[23, 65]	[24, 67]	[29, 66]	[21, 63]	[1, 82]
r_c	[170, 205]	[170, 205]	[170, 205]	[170, 205]	[165, 205]
ρ_s	[900, 1000]	[900, 1000]	[900, 1000]	[900, 1000]	[900, 1000]
ρ_o	[950, 1100]	[950, 1100]	[975, 1100]	[950, 1100]	[950, 1100]
ρ_c	[2158, 2829]	[2158, 2829]	[2166, 2829]	[2158, 2829]	[2156, 2946]
$\rho_o - \rho_s$	[0, 200]	[0, 200]	[75, 200]	[0, 200]	[0, 200]

interfaces can be described by triaxial ellipsoids. The radial distance $r_i(\theta, \phi)$ of a point on interface i with co-latitude θ and longitude ϕ can be expressed as

$$r_i(\theta,\phi) = r_i^0\left[1 - \frac{2}{3}\alpha_i P_2(\cos\theta) + \frac{1}{6}\beta_i P_2^2(\cos\theta)\cos 2\phi\right], \quad (3)$$

where $r_i^0 = a_i(1 - \alpha_i/3 - \beta_i/2)$ is the mean radius of interface i given by the spherically symmetric reference model, $\alpha_i = [(a_i + b_i)/2 - c_i]/[(a_i + b_i)/2]$ is the polar flattening and $\beta_i = (a_i - b_i)/a_i$ the equatorial flattening. Here, a_i, b_i, and c_i are the semi-major axes of the ellipsoid and $P_2(\cos\theta)$ and $P_2^2(\cos\theta)$ are the associated Legendre functions. The interface of the core is denoted by c for core, the interface between the ocean and the shell by o for ocean, and the outer surface by s for shell. We use different assumptions to calculate the flattenings. First, in Sections 3.1 and 3.2, we consider that Enceladus is in hydrostatic equilibrium and calculate the polar and equatorial flattening of the interfaces by solving Clairaut's equation for the synchronously rotating satellite (see e.g. Hubbard et al., 1984; Moritz, 1990; Van Hoolst et al., 2008). Second, we use the topography and gravity data (Iess et al., 2014; Nimmo et al., 2011; Thomas et al., 2016) at degree two to calculate the non-hydrostatic flattenings of the interfaces for two different assumptions on the compensation mechanism (Section 3.3). The flattening values are shown in Fig. 1.

For large icy satellites such as Titan and the Galilean icy satellites, the libration amplitude of the shell g_s can be well approximated by

$$g_s \approx \frac{4eK_3}{n^2 C_s} \quad (4)$$

(Van Hoolst et al., 2013). Here C_s is the polar moment of inertia of the shell and K_3 is the effective strength of the total diurnal forcing torque exerted on the shell. It essentially consists of the sum of the gravitational torque exerted by Saturn and of the associated pressure torque exerted by the ocean, both on the static shape of the shell of Enceladus and the tidal bulge of the shell (see Van Hoolst et al., 2013 for explicit expressions), other terms contributing about 1% or less (for models with a shell thickness above 15 km).

For the models of the interior structure of Enceladus considered here and for a flattening profile consistent with hydrostatic equilibrium, the shell has a considerably smaller moment of inertia than the entire satellite, between 6% and 63% of the total moment of inertia for shells with increasing thickness from 5 km to 72 km. The total torque on the shell is between 61% and 79% of the total torque on the entire satellite. The relative reduction in the total torque on the shell with respect to the torque on the entire satellite is therefore much less than the relative reduction in the polar moment of inertia of the shell with respect to that of the entire satellite, in particular for thin shells. As a result, the comparison of Eqs. (1) and (4) shows that the libration of the shell above a global ocean is larger than the libration if Enceladus were not to have a global decoupling ocean. We note that in sharp contrast to the large icy satellites for which tidal deformation can reduce the planet torque on the shell by up to one order of magnitude for thin shells, the torques related to the tidal deformation of Enceladus decrease the total torque on the shell with respect to a rigid satellite by 11% at most for the models with the thinnest shell as a result of the much smaller tidal deformation. For a shell thickness of 20 km, the reduction is at most 3%.

The libration amplitude is further increased by a resonance with a free mode, in particular for thin shells. Two free libration modes exist for a satellite with a global subsurface ocean: (1) an in-phase libration of the solid core and shell, (2) an out-of-phase libration (Van Hoolst et al., 2013). The period of the first mode is close to that for an entirely solid satellite since the ocean is thin (Fig. 2), justifying neglecting the square of this free frequency with respect to n^2, as done in Eq. (4). The period of the second mode decreases from about 4.7 days to about 1.5 days, close to the orbital forcing period, for shell thicknesses decreasing from 72 km to 5 km (Fig. 2). We therefore extend approximation (4) for the libration amplitude to

$$g_s \approx \frac{4eK_3}{C_s(n^2 - K_1/C_s)}. \quad (5)$$

Here, the square of the second free frequency is approximated by K_1/C_s, as follows from Eq. (64) of Van Hoolst et al. (2013), see also their Eq. (47) for the definition of the coupling strength K_1. The ratio of K_1/C_s to n^2 increases from 0.08 to 0.78 for shell thickness decreasing from 72 km to 5 km, showing that the amplitude of libration can increase by a factor of up to 4 for the thinnest shells as a result of the resonance with the second free mode.

In Fig. 2, the libration amplitude is represented for all interior structure models of Enceladus. The libration amplitude strongly depends on the thickness of the ice shell. For a shell rigidity of 3.3×10^9 Pa (Shoji et al., 2013), only models with a mean shell thickness in the range [16,23] km are consistent with the observed libration amplitude at the equatorial surface of Enceladus of [466, 590] m (2σ uncertainty of Thomas et al., 2016), see Fig. 2. Thomas et al. (2016) concluded that the ice shell must be on average between 21 km and 26 km thick based on the libration model of Van Hoolst et al. (2009) for rigid solid layers, about 4 km thicker than our result. The difference is not due to elasticity, since the range for rigid solid layers is extended by only 1 km to [16, 24] km, but mainly due to the different sampling of the interior structure models. If the ocean would have a high salinity ($\rho_o >$ 1100 kg/m^{-3} and up to $\rho_o = 1200$ kg/m^{-3}) due to exchange with the underlying core or if the shell would have a high porosity (850 kg/m$^{-3} < \rho_s <$ 900 kg/m^{-3}), the thickness of the shell could be up to 26 km, a value corresponding to the upper limit given by Thomas et al. (2016), who consider very low densities of the ice

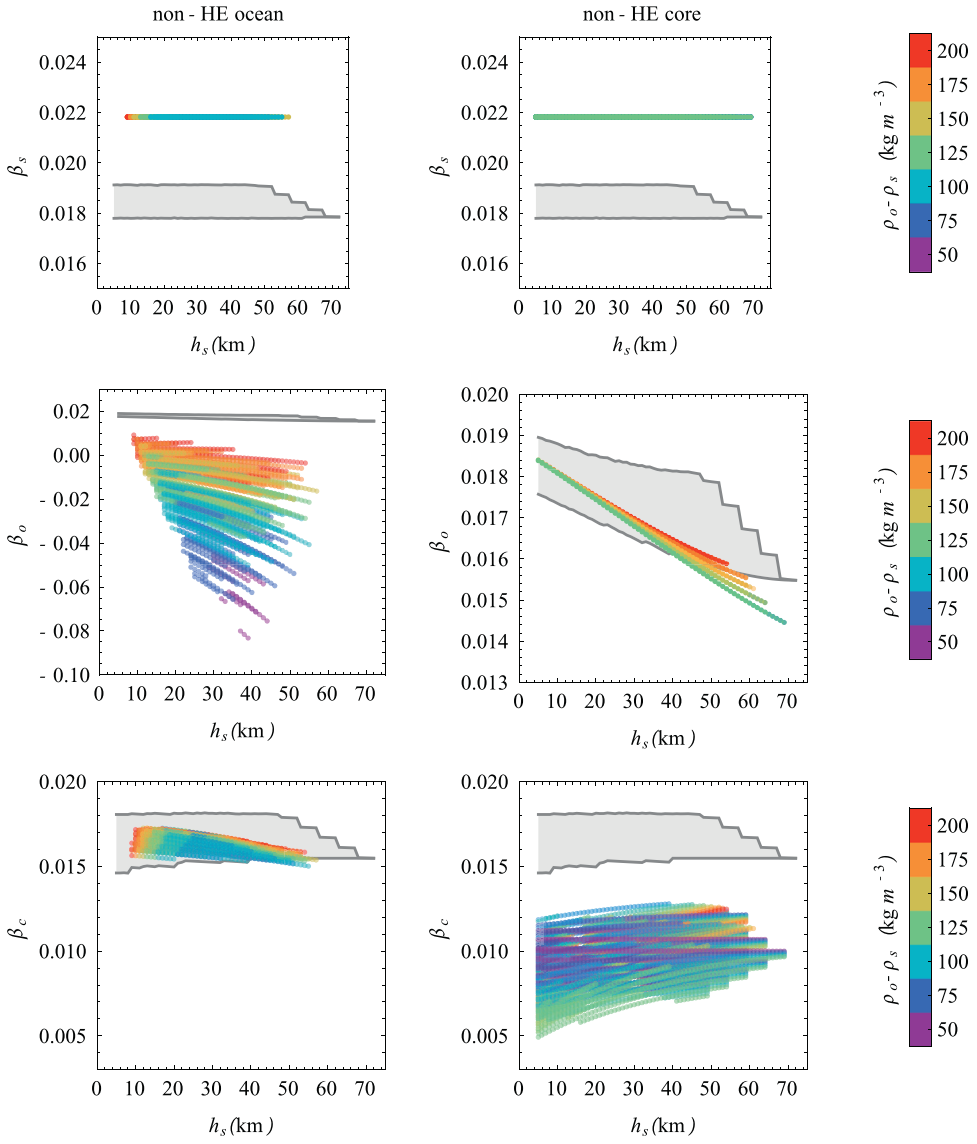

Fig. 1. Equatorial flattenings of the surface (top), ocean-shell interface (middle) and core (bottom) for the interior structure models of Enceladus as a function of the shell thickness. Three cases are considered: hydrostatic equilibrium (in grey), a non-equipotential ocean-shell interface (left), and a non-equipotential core-ocean interface (right). The scale of the vertical axes is not always the same. (For interpretation of the references to color in this figure legend, the reader is referred to the web version of this article.)

shell. The lower limit we obtain for the mean thickness of the ice shell is also due to our wider sampling in which we also consider small density differences between the ocean and the shell. We note that the surface flattenings in Thomas et al. (2016) correspond to those of the observed topography, and are therefore not hydrostatic. Since the flattenings of the internal interfaces depend on the non-hydrostatic surface flattenings in the calculation of Thomas et al. (2016) (see their Eqs. (15) and (16)), the internal flattenings cannot be truly hydrostatic flattenings. By convention, hydrostatic flattenings describe the degree-two shape of equipotential surfaces related to self-gravity, the centrifugal potential and the static tidal potential (Hubbard et al., 1984; Moritz, 1990). As such they cannot depend on non-hydrostatic surface flattenings. Since the observed equatorial surface flattening of Thomas et al. (2016) ($\beta_s = 0.0187 \pm 0.0007$) almost overlaps the range [0.0178, 0.0191] of hydrostatic flattenings for our set of interior structure models, the effect on the ice shell thickness is nevertheless below 1 km.

Because of the different flattenings of the surface and the interface between the ocean and ice shell, the thickness of the ice shell is variable. Fig. 3 shows the ice shell thickness as a function of co-latitude and longitude for a model with a mean shell thickness of 20 km that satisfies the observed libration amplitude. Since we here consider hydrostatic equilibrium and the shell is thin, the flattenings of the surface and of the interface between the ocean and the shell are very similar (see Fig. 1). As a result, the variations in the shell thickness are small and less than 1 km (Fig. 3). This may seem surprising since both the activity and the gravity and topography data indicate that the shell is much thinner at the south pole than elsewhere. We will show in Section 3.3. that much larger variations in the shell thickness and a much thinner shell at the south pole is possible when we relax the assumption of hydrostatic equilibrium and take into account the gravity and topography data.

3.2. Effect of ice rigidity and viscosity

In Fig. 2, the rigidity of the ice shell is fixed to 3.3×10^9 Pa, close to the value of Helgerud (2009) at zero pressure and zero degree Celsius, and the rigidity of the core is taken to be 50×10^9 Pa. The rigidity of the core has a negligible effect on the libration due

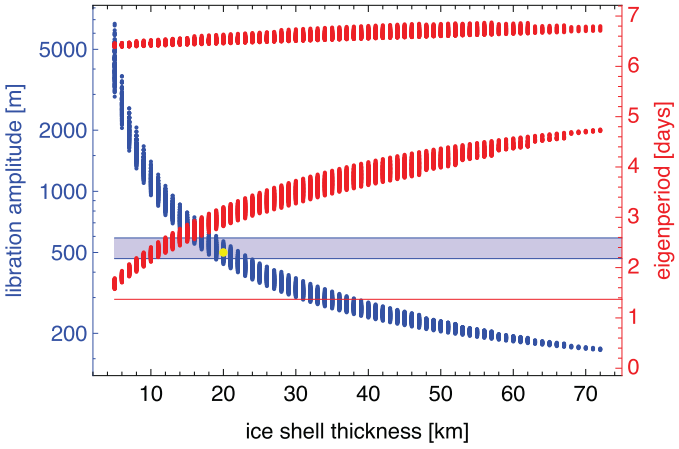

Fig. 2. Amplitude of libration of the ice shell and periods of the two free libration modes as a function of shell thickness. Shell rigidity is 3.3×10^9 Pa and the rigidity of the core is 50×10^9 Pa. We here assume that the shape of the interfaces between the different layers is determined from the reaction of a hydrostatic satellite to the centrifugal and static tidal potentials. The amplitude calculated with the approximated solution (4) differs from the amplitude represented here and obtained by solving the full set of equations governing libration as determined in Van Hoolst et al. (2013) by less than 0.9%. The period of the in-phase mode has a nearly constant value close to that for an entirely solid Enceladus (5.81 days). For shell thicknesses decreasing from 72 km to 5 km, the period of the out-of-phase mode period decreases from about 4.7 days to about 1.5 days, close to the orbital forcing period of 1.37 days (red line), allowing a resonant amplification of the libration amplitude which increases with decreasing shell thickness. For thick ice shells, the libration amplitude is close to the libration of a solid Enceladus (132 m). Only models with a shell thickness in the range [16, 23] km are consistent with the observed libration amplitude at the equatorial surface of Enceladus of [466, 590] m (blue region). The yellow marker (•) denotes the model used in Figs. 3 and 4, which has a mean shell thickness of 20 km. Models for non-hydrostatic shapes and other shell rigidity and viscosity values show a qualitatively similar dependence on the mean thickness of the ice shell. (For interpretation of the references to color in this figure legend, the reader is referred to the web version of this article.)

to the much smaller tidal displacement of the core below the subsurface ocean than of the ice shell. Here we consider nominal shell ice rigidity values between 10^9 Pa and 5×10^9 Pa. Lower values for the rigidity are not impossible but require substantial porosity of the ice (e.g. Wahr et al., 2006). The libration amplitude increases by about 10 % (50 m) over this range (Fig. 4), from low to high ice rigidity. For rigidity values within the nominal range the thickness estimate of the ice shell only marginally changes to [14, 24] km (Table 1). Shell rigidities below 10^8 Pa are not consistent with the observed libration amplitude since the predicted amplitude for all models is then below the lowest limit of the observations (shells thinner than 5 km would be required to resonantly increase the amplitude to the observed range).

Viscosity of the ice reduces the libration amplitude (Jara-Orué and Vermeersen, 2014). We extend the libration model of Van Hoolst et al. (2013) to include visco-elastic deformation by calculating the tidal deformation and Love numbers for a visco-elastic rheology. We describe the complex, frequency-dependent rigidity μ_s of the shell for a Maxwell model by

$$\mu_s(n) = i\frac{n\mu\eta}{\mu + in\eta}, \tag{6}$$

where i is the imaginary number, μ the real rigidity of the ice shell, and η the ice viscosity (e.g. Tobie et al., 2005; Vermeersen and Sabadini, 2004). Since viscosity strongly depends on temperature, we take a larger viscosity (larger than 10^{15} Pa s) for the cold top layer than for the hotter bottom layer of the ice shell (total temperature difference of about 180 K). We assume that the bottom half of the ice is convecting and has a nearly constant temperature, whereas in the top half heat is transported by conduction. The bottom ice is considered to have a viscosity close to the melting point viscosity between 10^{13} Pa s and 10^{15} Pa s (value depending on the grain size, Sotin et al., 2009). The libration amplitude does not depend on the exact value of the top viscosity because the top ice behaves elastically for the Maxwell model considered. The Maxwell timescale, separating elastic from fluid behavior, corresponds to the libration period for a viscosity of 3.9×10^{14} Pa s for the nominal rigidity value. The libration amplitude is almost constant for bottom viscosities between 10^{14} Pa s and 10^{15} Pa s, decreases due to more fluid-like behavior with decreasing bottom viscosity between 10^{14} Pa s and 10^{13} Pa s and is almost constant for viscosities smaller than 10^{13} Pa s (Fig. 4). The variation in libration amplitude is less than 20 m over the nominal viscosity range considered, well below the observational precision of Thomas et al. (2016). We conclude that the uncertainty in the ice viscosity does

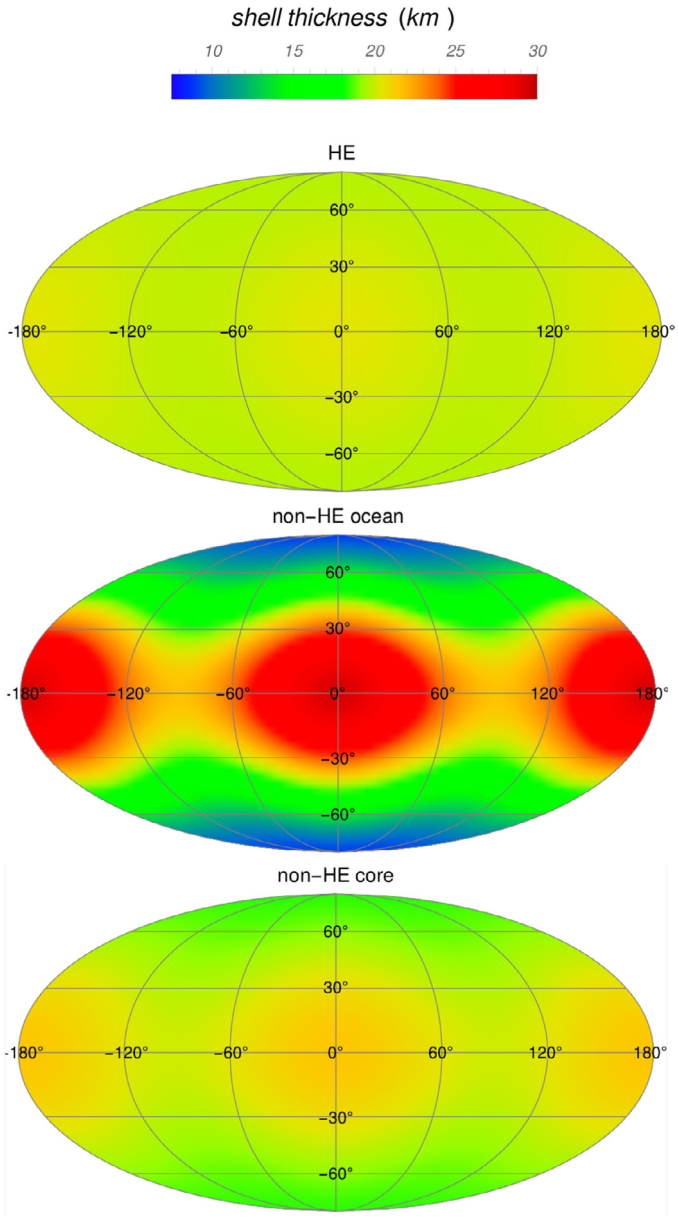

Fig. 3. Map of the local thickness of the ice shell for hydrostatic equilibrium (top), a non-equipotential ocean-shell interface (middle), and a non-equipotential core-ocean interface (bottom) for an interior structure model of Enceladus with shell thickness of 20 km, shell density of 925 kg m^{-3}, ocean density of 1050 kg m^{-3}, and core radius of 190 km, shown in Fig. 2 by a yellow marker (•). (For interpretation of the references to color in this figure legend, the reader is referred to the web version of this article.)

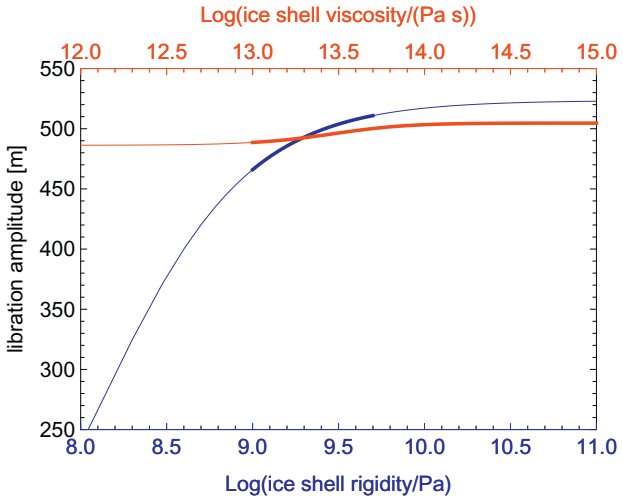

Fig. 4. Amplitude of libration as a function of shell rigidity (blue) and bottom shell viscosity (red) for an interior structure model of Enceladus with shell thickness of 20 km, shell density of 925 kg m^{-3}, ocean density of 1050 kg m^{-3}, and core radius of 190 km, shown in Fig. 2 by a yellow marker (•) Viscosity is neglected for the study of the dependence on shell rigidity and rigidity is set to 3.3 GPa for the study of the dependence on shell viscosity. Only bottom shell viscosity is varied, top viscosity is set to 10^{15} Pa s. Thick lines indicate results for nominal values of rigidity and bottom ice viscosity. (For interpretation of the references to color in this figure legend, the reader is referred to the web version of this article.)

not affect the interpretation of the libration amplitude in terms of the shell thickness at the level of precision of the observations.

3.3. Effect of non-hydrostatic structure

Measurements of the gravity field and topography of Enceladus by the Cassini spacecraft during close flybys show that Enceladus deviates from hydrostatic equilibrium. The second-degree gravity coefficients (C_{22} and $J_2 = (5435.2 \pm 34.9) \times 10^{-6}$) yield a ratio $J_2/C_{22} = 3.51 \pm 0.05$ (Iess et al., 2014) that is significantly larger than the value of about 3.25 expected for a hydrostatic Enceladus rotating at its current rotation speed (McKinnon, 2015). Also the ellipsoidal shape of Enceladus as derived from limb profiles is incompatible with hydrostatic equilibrium (Nimmo et al., 2011).

A non-hydrostatic shape of the outer surface affects the libration of Enceladus by changing the principal moments of inertia of the ice shell and therefore also the torques exerted on the shell. In addition to a non-hydrostatic shape of the surface, also the other interfaces (core-ocean and ocean-shell) can be of a non-hydrostatic shape, further modifying the libration. We assume here that the density within each layer is homogeneous. The observed gravity coefficients J_2 and C_{22} can then only be explained by assuming that at least one of the internal interfaces has a non-hydrostatic shape. We here consider two extreme cases: either (1) we explain the degree-two gravity coefficients by assuming that the bottom of the ice shell is not an equipotential surface or (2) we assume that the interface between the core and the ocean does not correspond to an equipotential surface. The other surface is assumed to be an equipotential surface of the self-gravitational potential, the centrifugal potential and the static tidal potential. We determine the equatorial and polar flattenings of both surfaces by solving four equations. Two equations express that one interface is equipotential in its degree-two, order-zero and its degree-two, order-two components, the other two equations express that the degree-two, order-zero and the degree-two, order-two gravity coefficients are equal to their observed values. In the first case of compensation through shell thickness variations, we have

$$\frac{2}{3}\alpha_c r_c^0 g_c = \frac{5}{6}n^2 (r_c^0)^2 + \frac{8\pi G}{15}\big[\alpha_s\rho_s + \alpha_o(\rho_o - \rho_s) + \alpha_c(\rho_c - \rho_o)\big](r_c^0)^2, \tag{7}$$

$$\frac{1}{6}\beta_c r_c^0 g_c = \frac{1}{4}n^2 (r_c^0)^2 + \frac{2\pi G}{15}[\beta_s\rho_s + \beta_o(\rho_o - \rho_s) + \beta_c(\rho_c - \rho_o)](r_c^0)^2, \tag{8}$$

where g_c is the local gravity at the core interface, and

$$C_{20} = -\frac{1}{M_E R^2}\frac{8\pi}{15}\big[\rho_s(R^5\alpha_s - (r_o^0)^5\alpha_o) + \rho_o((r_o^0)^5\alpha_o - (r_c^0)^5\alpha_c) + \rho_c(r_c^0)^5\alpha_c\big], \tag{9}$$

$$C_{22} = \frac{1}{4M_E R^2}\frac{8\pi}{15}\big[\rho_s(R^5\beta_s - (r_o^0)^5\beta_o) + \rho_o((r_o^0)^5\beta_o - (r_c^0)^5\beta_c) + \rho_c(r_c^0)^5\beta_c\big], \tag{10}$$

(see also Baland et al., 2014). For the second case in which we assume that the core-ocean interface is not an equipotential surface, we calculate the flattenings by solving Eqs. (11) and (12) together with

$$\frac{2}{3}\alpha_o r_o^0 g_o = \frac{5}{6}n^2 (r_o^0)^2 + \frac{8\pi G}{15}\left\{[\alpha_s\rho_s + \alpha_o(\rho_o - \rho_s)](r_c^0)^2 + \alpha_c(\rho_c - \rho_o)\frac{(r_c^0)^5}{(r_o^0)^3}\right\}, \tag{11}$$

$$\frac{1}{6}\beta_o r_o^0 g_o = \frac{1}{4}n^2 (r_o^0)^2 + \frac{2\pi G}{15}\left\{[\beta_s\rho_s + \beta_o(\rho_o - \rho_s)](r_c^0)^2 + \beta_c(\rho_c - \rho_o)\frac{(r_c^0)^5}{r_o^0)^3}\right\}, \tag{12}$$

where g_o is the local gravity at the ocean-shell interface. The degree-two shape of the surface is taken from Nimmo et al. (2011). These models are therefore compatible with both the observed long wavelength topography and the degree-two gravity. We also considered the degree-two shape of Thomas et al. (2016), but only quote here the results obtained for the values of Nimmo et al. (2011) since those differ more from hydrostatic equilibrium than the values of Thomas et al. (2016).

We adapt the libration model of Van Hoolst et al. (2013) developed for hydrostatic equilibrium to non-hydrostatic interiors by replacing the flattenings by their non-hydrostatic values in all the equations. We only retain models for which the shell (ocean) thickness in any direction is at least 2.5 km (1 km). In case (1), the non-hydrostatic structure almost does not change the estimate of the thickness of the ice shell (Table 1) although the libration amplitude of individual models that satisfy the observed libration amplitude can be up to 160 m smaller with respect to the corresponding models in hydrostatic equilibrium for nominal ice rigidity values. The assumption of a non-equipotential core boundary shifts the interval of possible ice shell thicknesses compatible with the observed libration amplitude to larger values of [18, 26] km. The libration amplitude of the individual models is between 49 m and 129 m larger with respect to the hydrostatic models.

Fig. 3 shows the large effect of the non-hydrostatic models on the local ice shell thickness. The results are illustrated for one interior structure model with a mean shell thickness of 20 km that satisfies the observed libration amplitude. The south polar region is only a few kilometer thick compared to thicknesses of over 30 km in the equatorial regions when it is assumed that the interface between the ocean and the shell is a non-equipotential surface. Within this compensation model, the small density contrast between the shell and the ocean leads to pronounced variations in

the position of the ocean-shell interface with an interface closer to the surface at topographic lows such as the south pole region, as can be seen from the negative sign of the equatorial flattening of the ocean-shell interface in Fig. 1 (see also Fig. 5 of the thickness of the shell and ocean in McKinnon, 2015). The local thicknesses shown in Fig. 3 are based on the degree-two shapes of the surface and the ocean-shell interface. This implies that the north polar region has an equally thin shell. Higher-degree components of the shape will affect these estimates, but have no influence on the libration amplitude (see Section 3.1). When the interface between the core and the ocean is considered to be a non-equipotential surface, the variations in the thickness of the ice shell are much smaller because of the larger density contrast of the core with the H_2O layer, and of the order of 3 km. Only for a non-equipotential ocean-shell interface can the shell be below 10 km thick. For the nominal range in ice shell rigidity ([1, 5] GPa), the thickness of the shell at the south pole is then between 2.5 km and 17 km.

4. Discussion and conclusions

We confirm and strengthen the results of Thomas et al. (2016) that the observed libration amplitude at orbital period is evidence of a global subsurface ocean. The existence of a global ocean has also been suggested on the basis of gravity and topography data (McKinnon, 2015) and is also consistent with the observed orbital modulation of the plume brightness due to tides (Behounková et al., 2015). Those studies predict an ice shell thickness of about 50 km or more and a thin ocean less than 20 km thick. The libration amplitude suggests the opposite: a thin shell with a thicker ocean. Although the gravity and topography data are very useful, and are also used in our analysis of the libration, it must be kept in mind that their interpretation in terms of the thickness of the shell is based on several uncertain assumptions. In the analyses of Iess et al. (2014) and McKinnon (2015), Airy isostasy is assumed. In such a model, the mass within any column of matter above the compensation depth is considered to be the same and due to local thickening or thinning of the ice shell. Compensation, however, can also be due to elastic and dynamic support (Wieczorek, 2015). Depending on the physical origin of the mass anomalies, the shell thickness may be strongly different from what is assumed within the assumption of Airy isostasy. Note also that the lowest-degrees two and three are used, for lack of higher degree gravitational data, and those can be more strongly influenced by the deeper interior than higher degrees.

Table 1 summarizes the mean thicknesses of the shell and ocean for different modeling hypotheses and model parameter ranges. The results show that the libration amplitude implies that the ice shell (ocean) is between 14 km and 24 km (24 km and 67 km) thick for both hydrostatic models and models that satisfy the observed degree-two gravity and topography by a non-equipotential ocean-shell interface. If instead, topography and gravity would be due to a non-equipotential core boundary, the shell (ocean) thickness is between 18 km and 26 km (21 km and 63 km). Other parameters of the interior structure are not constrained by the libration. The thickness of the shell at the south pole is between 2.5 km and 17 km (16.4 km and 24.3 km) for the non-hydrostatic models with non-equipotential ocean-shell (core-ocean) interface. These thickness variations are based only on the degree-two components of the shape of the surface and of the ocean-shell interface.

Thicker shells could be possible for larger density contrasts between the ice and the ocean than considered here. For example, for ocean densities up to 1200 kg/m^3, the upper limit for the mean thickness of the ice shell increases by 3 km for the interior structure models in hydrostatic equilibrium with the reference value of the rigidity of the ice shell. A lower-density ice shell also increases the mean shell thickness corresponding to the observed libration amplitude since it increases the libration amplitude. For example, for an extreme case with a shell porosity of about 50% (densities considered between 450 and 500 kg/m^3), the mean thickness of the shell can be up to 34 km for hydrostatic models. Such a high porosity can decrease the rigidity by about an order of magnitude (Hessinger et al., 1996). Since a decrease in the shell rigidity also decreases the libration amplitude (see Fig. 4) the mean shell thickness corresponding to the observed libration amplitude will be smaller than 34 km when we take into account this reduction in ice rigidity. When we take a rigidity value of 0.33 GPa, the mean thickness of the ice shell can be up to 31 km.

Acknowledgments

RMB is funded by a FSR grant from UCL, AT received financial support of the Belgian PRODEX program managed by the European Space Agency in collaboration with the Belgian Federal Science Policy Office.

References

Baland, R.M., Tobie, G., Lefèvre, A., et al., 2014. Titan's internal structure inferred from its gravity field, shape, and rotation state. Icarus 237, 29–41.
Baland, R.-M., Yseboodt, M., Van Hoolst, T., 2016. The obliquity of enceladus. Icarus 268, 12–31.
Behounková, M., Tobie, G., Cadek, O., et al., 2015. Timing of water plume eruptions on Enceladus explained by interior viscosity structure. Nat. Geosci. 8, 601–604.
Dehant, V., Mathews, P.M., 2015. Precession, Nutation, and Wobble of the Earth. Cambridge University Press, UK.
Hedman, M.M., Gosmeyer, C.M., Nicholson, P.D., et al., 2013. An observed correlation between plume activity and tidal stresses on enceladus. Nature 500, 182.
Helgerud, M.B., Waite, W.F., Kirby, S.H., et al., 2009. Elastic wave speeds and moduli in polycrystalline ice Ih, sI methane hydrate, and sII methane–ethane hydrate. J. Geophys. Res. 114, B02212.
Hessinger, J., White, B.E., Pohl, R.O., 1996. Elastic properties of amorphous and crystalline ice films. Planet. Space Sci. 44, 937–944.
Hsu, H.W., Postberg, F., Sekine, Y., et al., 2015. Ongoing hydrothermal activities within enceladus. Nature 519, 207210.
Hubbard, W.B., Waite, W.F., Kirby, S.H., 1984. Planetary Interiors. Van Nostrand, New York.
Hurford, T.A., Helfenstein, P., Hoppa, G.V., et al., 2007. Eruptions arising from tidally controlled periodic openings of rifts on enceladus. Nature 447, 292.
Iess, L., Stevenson, D.J., Parisi, M., et al., 2014. The gravity field and interior structure of enceladus. Science 344, 78–80.
Jara-Orué, H.M., Vermeersen, B.L.A., 2014. The forced libration of Europa's deformable shell and its dependence on interior parameters. Icarus 229, 31–44.
McKinnon, W.B., 2015. Effect of Enceladus's rapid synchronous spin on interpretation of Cassini gravity. Geophys. Res. Lett. 42 (7), 2137–2143.
Moritz, H., 1990. The Figure of the Earth. Herbert Wichmann Verlag GmbH, Karlsruhe.
Nimmo, F., Bills, B.G., Thomas, P.C., 2011. Geophysical implications of the long-wavelength topography of the Saturnian satellites. J. Geophys. Res. 116, E11.
Nimmo, F., Porco, C., Mitchell, C., 2014a. Tidally modulated eruptions on Enceladus: CASSINI ISS observations and models. Astrophys. J. 148, 46.
Nimmo, F., Porco, C., 2014b, Encyclopedia of the solar system. In: Spohn, T., Breuer, D., Johnson, T.V. (Eds.). Elsevier, pp. 851–860.
Porco, C., DiNino, D., Nimmo, F., 2014. How the geysers, tidal stresses, and thermal emission across the south polar terrain of enceladus are related. Astrophys. J. 148, 45.
Porco, C.C., Helfenstein, P., Thomas, P.C., et al., 2006. Cassini observes the active south pole of enceladus. Science 311, 1393–1401.
Postberg, F., Kempf, S., Schmidt, J., et al., 2009. Sodium salts in e ring ice grains from an ocean below the surface of enceladus. Nature 459, 1098–1101.
Postberg, F., Schmidt, J., Hillier, J., et al., 2011. A salt-water reservoir as the source of a compositionally stratified plume on enceladus. Nature 474, 620–622.
Rambaux, N., Castillo-Rogez, J.C., Williams, J.G., et al., 2010. Librational response of enceladus. Geophys. Res. Lett. 37, L04202.
Sharqawy, M.H., Lienhard, J.H., Zubair, S.M., 2010. Thermophysical properties of seawater: A review of existing correlations and data. Desalination Water Treat. 16, 354?380.
Shoji, D., Hussmann, H., Kurita, K., et al., 2013. Ice rheology and tidal heating of enceladus. Icarus 226, 10–19.
Sotin, C., Tobie, G., Wahr, J., et al., 2009. Tides and tidal heating on Europa. In: Pappalardo, R.T., McKinnon, W.B., Khurana, K.K. (Eds.), Europa. University of Arizona Press, Tucson, pp. 85–117.
Spencer, J.R., Pearl, J.C., Segura, M., et al., 2006. Cassini encounters enceladus: Background and the discovery of a south polar hot spot. Science 311, 1401–1405.
Thomas, P.C., Tajeddine, R., Tiscareno, M.S., et al., 2016. Enceladuss measured physical libration requires a global subsurface ocean. Icarus 264, 37–47.

Tiscareno, M.S., Thomas, P.C., Burns, J.A., 2009. The rotation of janus and epimetheus. Icarus 204, 254–261. doi:10.1016/j.icarus.2009.06.023.
Tobie, G., Cadek, O., Sotin, C., 2008. Solid tidal friction above a liquid water reservoir as the origin of the south pole hotspot on enceladus. Icarus 196, 642–652.
Tobie, G., Mocquet, A., Sotin, C., 2005. Tidal dissipation within large icy satellites: Applications to Europa and titan. Icarus 177, 534?549.
Van Hoolst, T., Baland, R.M., Trinh, A., 2013. The effect of tides on the longitudinal librations of large synchronously rotating icy satellites. Icarus 226, 299–315.
Van Hoolst, T., Rambaux, N., Karatekin, O., et al., 2009. The effect of gravitational and pressure torques on titan's length-of-day variations. Icarus 200, 256–264.
Van Hoolst, T., Rambaux, N., Karatekin, O., et al., 2008. The librations, shape, and icy shell of Europa. Icarus 195/1, 386–399.
Vermeersen, B., Sabadini, R., 2004. Global Dynamics of the Earth. Kluwer Academic Publishers, Dordrecht.
Wahr, J.M., Zuber, M.T., Smith, D.E., et al., 2006. Tides on Europa, and the thickness of Europa's icy shell. J. Geophys. Res. 111, E12005. doi:10.1029/2006JE002729.
Wieczorek, M., 2015. Treatise on geophysics. 2nd edition. In: Gerald, S. (Ed.), Planets and Moons, vol. 10. Oxford: Elsevier. Section 10.05.